PHYSICAL REVIEW LETTERS

Accurate Evolutions of Orbiting Black-Hole Binaries without Excision

M. Campanelli,[1] C. O. Lousto,[1] P. Marronetti,[2] and Y. Zlochower[1]

[1]*Department of Physics and Astronomy, and Center for Gravitational Wave Astronomy, The University of Texas at Brownsville, Brownsville, Texas 78520, USA*
[2]*Department of Physics, Florida Atlantic University, Boca Raton, Florida 33431, USA*

We present a new algorithm for evolving orbiting black-hole binaries that does not require excision or a corotating shift. Our algorithm is based on a novel technique to handle the singular puncture conformal factor. This system, based on the Baumgarte-Shapiro-Shibata-Nakamura formulation of Einstein's equations, when used with a "precollapsed" initial lapse, is nonsingular at the start of the evolution and remains nonsingular and stable provided that a good choice is made for the gauge. As a test case, we use this technique to fully evolve orbiting black-hole binaries from near the innermost stable circular orbit regime. We show fourth-order convergence of waveforms and compute the radiated gravitational energy and angular momentum from the plunge. These results are in good agreement with those predicted by the Lazarus approach.

One of the most significant goals of numerical relativity is to compute accurate gravitational waveforms from astrophysically realistic simulations of merging black-hole binaries. The expectation of very strong gravitational wave emission from the merger of two black holes and some of the newest astrophysical observations, from supermassive galactic nuclei just about to merge [1] to stellar size black-hole binaries, make these systems one of the most extraordinary astrophysical objects under study today. Binary-black-hole mergers are expected not only to provide information about the history and formation of the binary system but also to provide important precise tests of strong-field, highly dynamical relativity.

Motivated by the forthcoming observations of ground-based gravitational wave detectors, such as the Laser Interferometer Gravitational-Wave Observatory [2], and by the next generation of space-based detectors, such as the Laser Interferometer Space Antenna [3], the numerical relativity community has dedicated a great deal of effort to solving the binary-black-hole problem over the last few decades. After the "binary-black-hole grand challenge," [4] several new approaches have been pursued in the attempt to produce stable three-dimensional (3D) numerical codes capable of evolving the full Einstein field equations in the absence of any symmetry. This includes the introduction of new formulations of these equations and the development of numerical techniques for accurate evolutions of black-hole binaries, such as higher-order finite differencing, spectral methods, and adaptive mesh refinement (see Ref. [5], and references therein).

The calculation of the gravitational radiation emitted from plunging black-hole binaries was pioneered through the use of the Lazarus approach, which bridges numerical relativity and perturbative techniques to extract approximate gravitational waveforms [6–8]. More recently, important progress has been made toward evolving orbiting binary-black-hole spacetimes with the use of stable full 3D

numerical relativity codes using corotating gauge conditions and singularity excision [9–11].

Here we present a novel technique for evolving orbiting black holes based on puncture data. This technique does not require a corotating shift or singularity excision. Most importantly, we can produce accurate complete waveforms from merging black-hole binaries.

In a previous paper, we presented techniques for successfully performing numerical relativity simulations of black-hole binaries with fourth-order accuracy [12]. Our simulations are based on a new coding framework, LAZEV, which is built on top of the CACTUS Computational Toolkit [13]; this currently supports higher-order finite differencing for the Baumgarte-Shapiro-Shibata-Nakamura (BSSN) formulation of Einstein's equations [14–16] but is designed to be readily applicable to a broad class of formulations. Highly accurate evolutions can be achieved using our unigrid higher-order finite-difference code along with a nonuniform coordinate system, such as "Fisheye" [8], that concentrates grid points in the central region containing the black holes.

In the puncture approach [17], the metric on the initial slice is given by [18] $\gamma_{ab} = (\psi_{\rm BL} + u)^4 \delta_{ab}$, where $\psi_{\rm BL} = 1 + \sum_{i=1}^{n} m_i/(2r_i)$ is the Brill-Lindquist conformal factor, m_i is the mass parameter of puncture i, r_i is the coordinate distance to puncture i, and u is finite on the punctures. If the puncture positions are fixed throughout the evolution, then the singular behavior in the metric is contained in $\psi_{\rm BL}$ and can, thus, be treated analytically. However, holding the puncture fixed throughout the evolution leads to significant coordinate distortions that tend to kill the run before a common horizon forms.

We propose a method for evolving puncture type data without fixing the puncture positions during the evolution. Our method is based on the BSSN formulation. In the BSSN system, one evolves a conformal metric $\tilde{\gamma}_{ab} = \exp(-4\phi)\gamma_{ab}$ which has unit determinant $K = K_a^a$, the

conformal trace-free extrinsic curvature $\tilde{A}_{ab} = \exp(-4\phi)(K_{ab} - \gamma_{ab}K/3)$, the conformal exponent ϕ, and $\tilde{\Gamma}^i = -\partial_j \tilde{\gamma}^{ij}$. In order to regularize the system near the puncture, we replace the BSSN exponent ϕ [which has an $O(\ln r)$ singularity at the puncture] with a new variable $\chi = \exp(-4\phi)$ that is C^4 on the puncture. Additionally, we modify the standard $1 + \log$ lapse and Gamma-driver shift gauge conditions [19]. Our system is explicitly finite on the initial slice. The evolution equations for this system are [14–16,19]

$$\partial_0 \tilde{\gamma}_{ij} = -2\alpha \tilde{A}_{ij}, \tag{1}$$

$$\partial_t \chi = \tfrac{2}{3}\chi(\alpha K - \partial_a \beta^a) + \beta^i \partial_i \chi, \tag{2}$$

$$\partial_0 \tilde{A}_{ij} = \chi(-D_i D_j \alpha + \alpha R_{ij})^{\mathrm{TF}} + \alpha(K\tilde{A}_{ij} - 2\tilde{A}_{ik}\tilde{A}^k_j), \tag{3}$$

$$\partial_0 K = -D^i D_i \alpha + \alpha(\tilde{A}_{ij}\tilde{A}^{ij} + \tfrac{1}{3}K^2), \tag{4}$$

$$\begin{aligned}
\partial_t \tilde{\Gamma}^i &= \tilde{\gamma}^{jk}\partial_j \partial_k \beta^i + \tfrac{1}{3}\tilde{\gamma}^{ij}\partial_j \partial_k \beta^k + \beta^j \partial_j \tilde{\Gamma}^i - \tilde{\Gamma}^j \partial_j \beta^i \\
&\quad + \tfrac{2}{3}\tilde{\Gamma}^i \partial_j \beta^j - 2\tilde{A}^{ij}\partial_j \alpha + 2\alpha(\tilde{\Gamma}^i_{jk}\tilde{A}^{jk} \\
&\quad + 6\tilde{A}^{ij}\partial_j \phi - \tfrac{2}{3}\tilde{\gamma}^{ij}\partial_j K),
\end{aligned} \tag{5}$$

where $\partial_0 = \partial_t - \mathcal{L}_\beta$, TF indicates that only the trace-free part of the tensor is used, $R_{ij} = \tilde{R}_{ij} + R^\phi_{ij}$ is given by

$$\begin{aligned}
R^\phi_{ij} &= -2\tilde{D}_i \tilde{D}_j \phi - 2\tilde{\gamma}_{ij}\tilde{D}^k \tilde{D}_k \phi + 4\tilde{D}_i \phi \tilde{D}_j \phi \\
&\quad - 4\tilde{\gamma}_{ij}\tilde{D}^k \phi \tilde{D}_k \phi,
\end{aligned} \tag{6}$$

$$\begin{aligned}
\tilde{R}_{ij} &= -\tfrac{1}{2}\tilde{\gamma}^{lm}\partial_l \partial_m \tilde{\gamma}_{ij} + \tilde{\gamma}_{k(i}\partial_{j)}\tilde{\Gamma}^k + \tilde{\Gamma}^k \tilde{\Gamma}_{(ij)k} \\
&\quad + \tilde{\gamma}^{lm}(2\tilde{\Gamma}^k_{l(i}\tilde{\Gamma}_{j)km} + \tilde{\Gamma}^k_{im}\tilde{\Gamma}_{klj}),
\end{aligned} \tag{7}$$

D_i is the covariant derivative with respect to γ_{ij}, and $\tilde{D}_i$ is the covariant derivative with respect to $\tilde{\gamma}_{ij}$. $\tilde{\Gamma}^i$ is replaced by $-\partial_j \tilde{\gamma}^{ij}$ in Eqs. (1)–(7) wherever it is not differentiated. Note that Eqs. (2) and (5) give the ∂_t derivatives of χ and $\tilde{\Gamma}^i$ rather than the ∂_0 derivatives. Note that $\partial_i \phi = -1/(4\chi)\partial_i \chi$ and $\partial_{ij}\phi = \tfrac{1}{4}(-\partial_{ij}\chi/\chi + \partial_i \chi \partial_j \chi/\chi^2)$ are singular on the puncture; as a result, we identify several potentially singular terms in Eqs. (1)–(5). In Eq. (3), the term $D_i D_j \alpha$ can be expressed in terms of $\partial_i \phi \partial_j \alpha +$ nonsingular terms. However, this term is multiplied by χ, and the product is C^3 on the puncture. Additionally, the $\partial_i \partial_j \phi$ terms (from R_{ij}) are multiplied by $\alpha\chi$ and are, thus, C^2 on the puncture. If the lapse $\alpha \sim r^2$ on the puncture (as is our choice), then $\tilde{A}_{ab}$ is C^4 on the puncture (provided that it is C^4 on the initial slice). However, in Eq. (5), we find the singular term $\alpha\tilde{A}^{ij}\partial_i \phi$. With our choice of initial data, $\tilde{A}^{ij} \sim r^2$, and, thus, $\tilde{\Gamma}^i$ is C^0 on the puncture. We can then choose an initial lapse $\alpha = \psi^{-2}_{\mathrm{BL}}$ which is $O(r^2)$ on the puncture. With this choice of lapse, $\tilde{\Gamma}^i$ evolves to a function that is C^2 on the puncture. However, $\tilde{\Gamma}^i$ will remain well behaved only if the lapse condition maintains

this $O(r^2)$ behavior near the puncture. We found that the following gauge conditions produced smooth waveforms:

$$\partial_0 \alpha = -2\alpha K, \tag{8}$$

$$\partial_t \beta^a = B^a, \qquad \partial_t B^a = 3/4\partial_t \tilde{\Gamma}^a - \eta B^a. \tag{9}$$

However, these gauge conditions require careful treatment of χ near the puncture in order for the system to remain stable. In particular, we enforce $\chi > \epsilon h^4$, where ϵ is chosen as small as possible.

In black-hole binary systems, the features that need to be resolved range in scale from a fraction of M near the horizons to over $100M$ in the wave zone when black holes are in a slow inspiral motion. This difference in scales makes simple unigrid evolutions extremely inefficient. We mitigate this problem by introducing a "multiple transition" Fisheye transformation. This Fisheye coordinate is a natural extension of the "transition Fisheye" coordinate [8,19] (where the effective resolution changes from some inner resolution h to an outer resolution ah inside a region of a given width, where a is a user specified parameter) but with multiple transition regions allowing for fine tuning of the resolution in intermediate regions. This new Fisheye coordinate simulates fixed-mesh refinement.

For puncture data, the estimated innermost stable circular orbit (ISCO) [20] is characterized by the parameters

$$\begin{aligned}
L/M &= 4.9, & P/M &= 0.335, & Y/M &= \pm 1.1515, \\
J/M^2 &= 0.77, & M\Omega &= 0.178, & m &= 0.45M, \quad (10)
\end{aligned}$$

where m is the mass of each single black hole, M is the total Arnowitt-Deser-Misner mass of the binary system, L is the proper distance between the apparent horizons, P is the magnitude of the linear momenta (equal but opposite and perpendicular to the line connecting the holes), J is the total angular momentum, and $(0, Y, 0)$ is the coordinate location of the punctures. We use the Brandt-Brügmann approach along with the BAM_ELLIPTIC [13,18] CACTUS thorn to solve for these initial data.

We use π-rotational symmetry about the polar axis (Pi symmetry) and reflection symmetry across the orbital plane to reduce the computational domain to one quadrant. We choose Fisheye parameters that produce an inner resolution h, an intermediate resolution of $5h$, and an outer resolution of $25h$. These parameters place the outer boundary at $88M$, where we use radiative boundary conditions on all variables [19].

At the puncture χ vanishes, and Eq. (2) implies that the puncture position obeys $\partial_t \vec{x}_{\mathrm{punct}} = -\vec{\beta}(\vec{x}_{\mathrm{punct}})$. We track the puncture positions throughout the evolution by integrating this equation (we confirmed that the coordinate location of the minimum value of χ is within one grid point of these integrated trajectories). Note that we stagger the grid about the $z = 0$ plane. Consequently, the punctures never lie on grid points. The shift at the punctures is obtained by fourth-order interpolation. Figure 1 shows
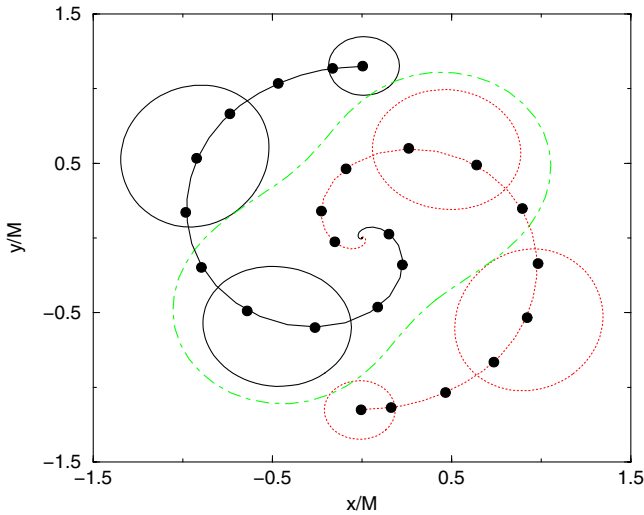
FIG. 1 (color online). The trajectories of the punctures along with the first common horizon and the individual horizons at $t = 0, 10M$, and $18.8M$. The solid circles correspond to the centroids of the apparent horizons every $2.5M$. The common horizon forms at $18.8M$, just before the puncture complete a half orbit. The punctures continue to orbit throughout the evolution.
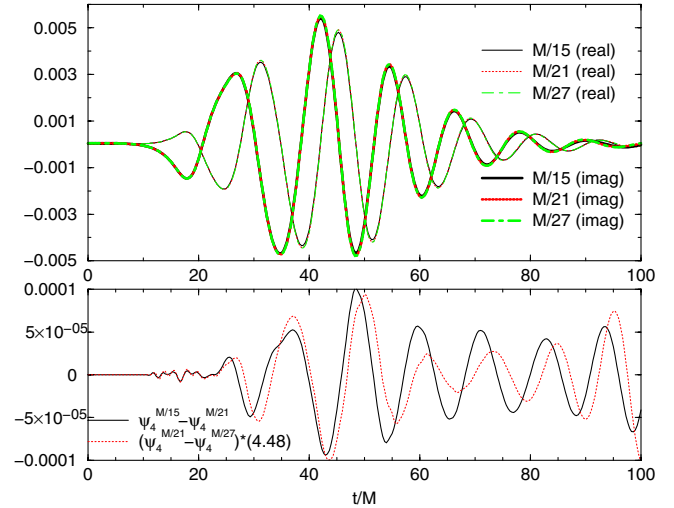

FIG. 2 (color online). QC0 waveforms. The top plot shows the real part (thinner lines) and imaginary part (thicker lines) of the $(\ell = 2, m = 2)$ mode of ψ_4 at $r = 15M$ for resolutions of $h = M/15, M/21$, and $M/27$. Note the $\pi/2$ phase lag in the real part. The bottom plot shows the differences between imaginary waveforms for $h = M/15$ and $h = M/21$ as well as the difference between waveforms for $h = M/21$ and $h = M/27$. The latter difference has been rescaled by 4.48 to demonstrate fourth-order convergence. The real part of the waveforms exhibits similar fourth-order convergence. Errors in the $M/27$ run are smaller than $1/200$ of the amplitude, as inferred by Richardson extrapolation, up to $t = 75M$.

the trajectory of the punctures for the $h = M/21$ run. A common horizon forms just before the punctures complete half of an orbit. The punctures continue to orbit throughout the evolution.

We use the ZORRO thorn [8,12] to calculate ψ_4 and decompose it into (ℓ, m) modes. Figure 2 shows the real and imaginary parts of the $(\ell = 2, m = 2)$ mode of ψ_4 at $r = 15M$ (we choose this small observer radius to delay outer boundary effects) for resolutions of $h = M/15$, $M/21, M/27$, as well as a convergence plot of these data. The lower plot shows that the waveforms are fourth-order convergent. The radiated energy (as measured from the $M/27$ run) is $2.8\% \pm 0.2\%$ in excellent agreement with the final horizon mass (see below), and the radiated angular momentum is $J_z = -0.12M^2 \pm 0.01M^2$ [computed using Eqs. (22)–(24) of Ref. [21]]. Our largest run ($h = M/27$) used $288^2 \times 576$ grid points (64 GB) and ran on 16 nodes (dual 3.2 GHz Xeon processors) for 2 weeks.

We use Thornburg's AHFINDERDIRECT thorn [22] to find apparent horizons. We first detect a common apparent horizon at $t = 18.8M$. The common horizon has an irreducible mass of $0.9056M$, and the ratio of polar to equatorial circumferences asymptotes to 0.900 ± 0.002. One can show analytically [9] that, for a Kerr black hole, the ratio of the polar and equatorial horizon circumferences $C_r = C_p/C_e$ is given by

$$C_r = \frac{1 + \sqrt{1 - \tilde{a}^2}}{\pi} E\left(-\frac{\tilde{a}^2}{(1 + \sqrt{1 - \tilde{a}^2})^2}\right), \qquad (11)$$

where $\tilde{a} = a/M_{\mathcal{H}}$ and $E(x)$ is the complete elliptic integral of the second kind. In the case of a perturbed black hole produced by a merger, this ratio shows quasinormal

ringing behavior before damping to the expected Kerr value. The horizon mass is related to the spin and irreducible mass by $M_{\mathcal{H}} = (M_{\mathrm{irr}}/\tilde{a})\sqrt{2(1 - \sqrt{1 - \tilde{a}^2})}$. Hence, the irreducible horizon mass and circumference ratio that we measure correspond to a spin of $\tilde{a} = 0.677 \pm 0.006$ and a horizon mass of $0.972M \pm 0.002M$. The horizon mass reduction is in excellent agreement with the calculated radiated energy of $0.028M \pm 0.002M$.

Table I summarizes the main results of our full numerical evolution of binary black holes from the ISCO down to the final Kerr black-hole remnant. Waveforms, as described in terms of the Weyl scalar ψ_4, are dominated by the modes $\ell = 2$, $m = \pm 2$ and show a strong circular polarization as seen along the axis of orbital symmetry. These results are in good agreement with the results calculated by the Lazarus approach [6,7]. The agreement is especially remarkable considering the vastly different approaches used.

TABLE I. Results of the evolution.

Method	E_{rad}/M	J_{rad}/M^2	t_{merger}/M	$a/M_{\mathcal{H}}$
This Letter	2.8 ± 0.2	$15 \pm 1\%$	$T_{\mathrm{CAH}} \approx 18.8$	0.677 ± 0.006
Lazarus[a]	2.5 ± 0.2	$13 \pm 2\%$	$T_{\mathrm{Tran}} \approx 10$	0.70 ± 0.02

[a]Errors quoted in the Lazarus runs are only those from the differences among transition times; hence, they represent only a lower bound to the total errors.
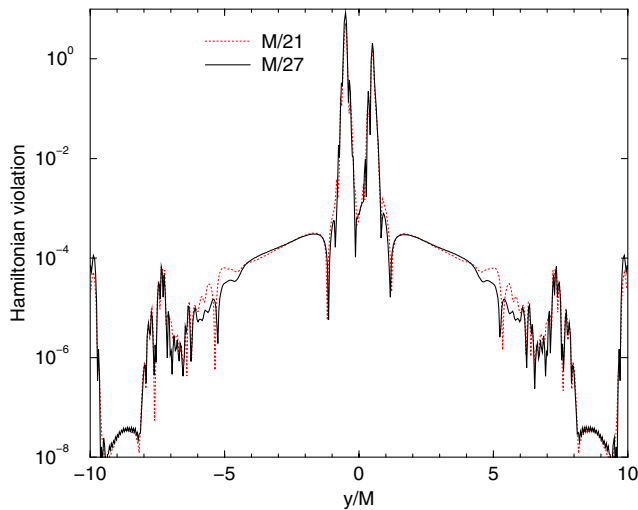
FIG. 3 (color online). The Hamiltonian constraint violation at $t = 22M$ along the y axis for $h = M/21$ and $h = M/27$ [rescaled by $(27/21)^3$]. The good agreement between these curves indicates that the Hamiltonian is third-order convergent. However, the constraint is linearly convergent on the puncture.

The Hamiltonian constraint violation is third-order convergent in the bulk, with linear convergence at the current puncture locations and fourth-order convergence at former puncture locations. Figure 3 shows the Hamiltonian constraint violation along the y axis at $t = 22M$ (approximately the time for half an orbit in this gauge).

Note that, in this Letter, we used a convenient numerical tetrad to calculate the Weyl scalar ψ_4. This waveform extraction procedure is valid when the far-field spacetime approaches that of a perturbed Schwarzschild black hole. In future simulations, we plan to use a more robust wave extraction method recently implemented in Ref. [23].

The full nonlinear numerical technique just described has shown long-term stability, at least for the merger of binary-black-hole cases we have had the opportunity to analyze so far. We have also been able to prove fourth-order convergence up to relatively high resolutions such as $h = M/36$. This opens up the possibility of studying even more interesting astrophysical scenarios such as black-hole binaries starting from larger separations, which would undergo several orbits before the final plunge. Additionally, we plan evolutions based on the more astrophysically relevant thin-sandwich [24] and post-Newtonian [25] initial data sets. We will also consider unequal-mass black-hole binaries and compute their gravitational kick in order to evaluate its astrophysical consequences [26]. Finally, we plan to examine mergers of highly spinning black-hole binaries and study the possible ''hangup'' of the binary until the excess angular momentum is radiated.

A similar approach to evolving moving black holes without excision has been independently implemented by Baker *et al.* [27]. Both techniques produce similar results for the emitted energy and radiated angular momentum.

[1] S. Komossa *et al.*, Astrophys. J. **582**, L15 (2003).
[2] R. Vogt, in *Proceedings of the Sixth Marcel Grossman Meeting on General Relativity, Kyoto, Japan, 1991*, edited by H. Sato and T. Nakamura (World Scientific, Singapore, 1992), pp. 244–266.
[3] K. Danzmann and A. Rudiger, Classical Quantum Gravity **20**, S1 (2003).
[4] http://www.npac.syr.edu/projects/bh/
[5] M. Alcubierre, gr-qc/0412019.
[6] J. Baker, M. Campanelli, C. O. Lousto, and R. Takahashi, Phys. Rev. D **65**, 124012 (2002).
[7] J. Baker, B. Brügmann, M. Campanelli, C. O. Lousto, and R. Takahashi, Phys. Rev. Lett. **87**, 121103 (2001).
[8] J. Baker, M. Campanelli, and C. O. Lousto, Phys. Rev. D **65**, 044001 (2002).
[9] M. Alcubierre *et al.*, Phys. Rev. D **72**, 044004 (2005).
[10] F. Pretorius, Phys. Rev. Lett. **95**, 121101 (2005).
[11] B. Brügmann, W. Tichy, and N. Jansen, Phys. Rev. Lett. **92**, 211101 (2004).
[12] Y. Zlochower, J. G. Baker, M. Campanelli, and C. O. Lousto, Phys. Rev. D **72**, 024021 (2005).
[13] http://www.cactuscode.org
[14] T. Nakamura, K. Oohara, and Y. Kojima, Prog. Theor. Phys. Suppl. **90**, 1 (1987).
[15] M. Shibata and T. Nakamura, Phys. Rev. D **52**, 5428 (1995).
[16] T. W. Baumgarte and S. L. Shapiro, Phys. Rev. D **59**, 024007 (1999).
[17] B. Brugmann, Int. J. Mod. Phys. D **8**, 85 (1999).
[18] S. Brandt and B. Brügmann, Phys. Rev. Lett. **78**, 3606 (1997).
[19] M. Alcubierre, B. Brügmann, P. Diener, M. Koppitz, D. Pollney, E. Seidel, and R. Takahashi, Phys. Rev. D **67**, 084023 (2003).
[20] T. W. Baumgarte, Phys. Rev. D **62**, 024018 (2000).
[21] M. Campanelli and C. O. Lousto, Phys. Rev. D **59**, 124022 (1999).
[22] J. Thornburg, Classical Quantum Gravity **21**, 743 (2004); URL http://stacks.iop.org/0264-9381/21/743.
[23] M. Campanelli, B. J. Kelly, and C. O. Lousto, gr-qc/0510122.
[24] M. D. Hannam, Phys. Rev. D **72**, 044025 (2005).
[25] W. Tichy, B. Brügmann, M. Campanelli, and P. Diener, Phys. Rev. D **67**, 064008 (2003).
[26] M. Campanelli, Classical Quantum Gravity **22**, S387 (2005).
[27] J. G. Baker, J. Centrella, D.-I. Choi, M. Koppitz, and J. van Meter, gr-qc/0511103.